Tectonics

RESEARCH ARTICLE
10.1029/2023TC007917

Key Points:

- The occurrence of XVI-century cascade in the Eastern Betic Shear Zone was encouraged by both coseismic and postseismic Coulomb stress changes
- Other faults including candidate causative faults for the 1658 Almeria Mw 6.2 earthquake have been loaded following the XVI-century cascade
- Postseismic viscoelastic effects on fault interaction should be integrated into fault-based and time-dependent seismic hazard assessments

Supporting Information:

Supporting Information may be found in the online version of this article.

Correspondence to:

P. Yazdi,
pouye.yazdi@upm.es

Citation:

Yazdi, P., García-Mayordomo, J., Álvarez-Gómez, J. A., Gaspar-Escribano, J. M., & Masana, E. (2023). Exploring the connection of XVI-century major historical earthquakes in the Eastern Betic Cordillera, Spain: Insights from viscoelastic relaxation of the lithosphere. *Tectonics*, *42*, e2023TC007917. https://doi.org/10.1029/2023TC007917

Received 5 MAY 2023
Accepted 25 OCT 2023

Author Contributions:

Conceptualization: Pouye Yazdi, Julián García-Mayordomo
Formal analysis: Pouye Yazdi, Jorge Miguel Gaspar-Escribano
Funding acquisition: Eulália Masana
Investigation: Pouye Yazdi, Julián García-Mayordomo
Methodology: Pouye Yazdi
Resources: Julián García-Mayordomo, Eulália Masana

Exploring the Connection of XVI-Century Major Historical Earthquakes in the Eastern Betic Cordillera, Spain: Insights From Viscoelastic Relaxation of the Lithosphere

Pouye Yazdi[1,2], Julián García-Mayordomo[2], José Antonio Álvarez-Gómez[3], Jorge Miguel Gaspar-Escribano[1], and Eulália Masana[4]

[1]Universidad Politécnica de Madrid, Madrid, Spain, [2]Instituto Geológico Minero de España (IGME), CSIC, Madrid, Spain, [3]Universidad Complutense de Madrid, Madrid, Spain, [4]Universitat de Barcelona, Barcelona, Spain

Abstract Understanding the crustal fault interaction and connection between earthquakes in areas with slow tectonic deformation, such as Betic Cordillera (South Spain), is challenging. When seismic rates are low and large destructive earthquakes happen less frequently, it is necessary to resort to historical or paleoseismic records. This study investigates the postseismic viscoelastic relaxation mechanism as a potential explanation for the occurrence of three historical earthquakes (I_{EMS}VIII-IX) in the Eastern Betic Shear Zone during the XVI-century, all of which occurred within a span of 13 years: 1518 Vera Mw6.2, 1522 Alhama de Almeria Mw6.5, and 1531 Baza Mw6.2 associated with the Palomares, Carboneras, and Baza faults, respectively. The results strongly suggest a sequential stress-triggering connection between the three events. The northern NS-oriented section of the Baza fault is found to have experienced a larger positive ΔCFS and, indeed, more prone to rupture in 1531. The study also examines whether the cumulative ΔCFS had influenced the occurrence of further significant earthquakes (≥Mw6.0) in the region. A triggering connection between the cascade and the 1658 Almeria Mw6.2 earthquake is suggested, whereas no indications of similar linkage to the 1674 Lorca Mw6.0 or the 1804 Dalias Mw6.4 events are found. The stress triggering impact of the cascade over nearby active faults is noteworthy. It is expected that this analysis could have future applications for studying other important historical events, and improving seismic hazard analysis in complex fault settings of the Betic Cordillera.

1. Introduction

The instrumental record for the Eastern Betic Shear Zone (EBSZ) indicates a relatively low-to-moderate seismic activity rate; nevertheless, this area has experienced large earthquakes throughout history (Figure 1). In the early XVI-century, three high-intensity destructive earthquakes caused massive damage and loss in several towns of southern areas in the EBSZ. These events remarkably occurred within a brief span of fewer than 13 years (between 1518 and 1531) and less than 90 km separation. Afterward, no similarly large earthquake (Mw ≥ 6.0) occurred in this area until the mid-XVII-century.

The occurrence of clusters of destructive events in history has been described frequently (e.g., Jia et al., 2023; Marco et al., 1996; Nur & Cline, 2000; Pondard et al., 2007; Zohar et al., 2017), and static stress changes are usually considered the mechanism driven this interaction (Stein et al., 1997). Stress changes of several bars are common after relevant earthquakes (e.g., Harris & Simpson, 1992; Parsons et al., 2008; Segou & Parsons, 2020; Toda & Stein, 2020), and changes as small as 0.1 bar are capable of triggering new events (Stein, 1999, and references therein). In the case of faults, with low slip-rates (<1 mm/yr), the stressing rate is lower than 0.01 bar/yr. In these cases 1 bar (0.1 MPa) of stress change imply a time advance of the nearby faults seismic cycle of hundreds or thousands of years (Martínez Díaz, Bejar-Pizarro, et al., 2012; Martínez Díaz, Masana, & Ortuño, 2012). Given that the EBSZ generally exhibits slow stress accumulation over its active faults, even minor changes in the distribution of stress could have a notable effect on when neighboring faults rupture. Accordingly, exploring the potential stress-triggering relationships among the three XVI-century earthquakes is essential for improving our understanding of long-term fault interactions within the slow tectonic stress buildup framework of the EBSZ. Furthermore, it could contribute to the seismogenic characterization of the fault system and seismic hazard assessments.

Software: Pouye Yazdi
Validation: Julián García-Mayordomo, José Antonio Álvarez-Gómez
Visualization: Pouye Yazdi
Writing – original draft: Pouye Yazdi, Julián García-Mayordomo
Writing – review & editing: Pouye Yazdi, Julián García-Mayordomo, José Antonio Álvarez-Gómez, Jorge Miguel Gaspar-Escribano

Coseismic stress changes can be permanent (static) and transient (dynamic). Both types can cause earthquake triggering (Belardinelli et al., 1999; Gomberg et al., 1998). At remote distances, the influence of coseismic transient stress becomes more dominant (Cotton & Coutant, 1997; Gomberg et al., 1998), and it is shown that it can trigger aftershocks for up to months (e.g., Hill et al., 1993; Kilb, 2000). On the other hand, the stress resulting from earthquake ruptures can induce further postseismic responses, including the afterslip that emerges as an aseismic slip, or even aftershocks, on the causing fault or its extensions (Freed, 2007; Marone et al., 1991). Another postseismic response occurs when the coseismic stress change in the brittle seismogenic layer (schizosphere) also transfers to the ductile deforming plastosphere (Scholz, 2019), where it relaxes through a viscoelastic postseismic process, allowing the effect to propagate over longer distances (Burgmann & Dresen, 2008; Rydelek & Sacks, 1990; Turcotte & Schubert, 2002). This relaxation occurs at a slow pace over decades, therefore the viscoelastic coupling between lithospheric layers can influence large earthquake interactions over a longer time scale (e.g., Freed & Lin, 2001; Nur & Mavko, 1974). In this study, only the effects of bulk viscoelastic relaxation are examined. Due to the absence of surface deformation data, accounting for possible contributions from afterslip and/or localized shear zones within the plastosphere (Jin et al., 2023; Scholz, 2019) is not feasible.

Estimating the Coulomb failure stress change (ΔCFS) is a well-established method to analyze the plausible stress-triggering influence between earthquakes (King et al., 1994; Nalbant et al., 1998; Toda et al., 2011). A positive correlation between earthquakes and zones of positive static coseismic ΔCFS has been shown in multiple studies (e.g., Deng & Sykes, 1996; Harris & Simpson, 1992; King et al., 1994; Reasenberg & Simpson, 1992; Stein, 1999). In the past two decades, several authors have used the combined (static and viscoelastic) ΔCFS estimation to explore the interaction between earthquakes within complex fault systems in long-term (e.g., Chëry et al., 2001; Freed et al., 2006; Liu et al., 2022; Marchandon et al., 2021; Rydelek & Sacks, 2001; Sunbul, 2019; Xiong et al., 2017). The combined ΔCFS expresses the effect of elastic rebound due to the static stress transfer and the viscoelastic relaxation in the less viscous lower crust and lithospheric mantle. For instance, Verdecchia et al. (2018) analyze several short-term and long-term earthquake cascades in the diffuse tectonic boundary along the Apennines (central Italy) and remark on the role of viscoelastic stress transfer due to events of Mw ≥ 6.5 on a centennial timescale to conclude that several faults may be close to failure at present. Unraveling the postseismic stress interactions in regions with low-to-moderate magnitude seismicity and very low deformation rates can be particularly challenging, as the size of the postseismic ΔCFS is impacted not just by the rheology parameters of the lithosphere but also by the magnitude of the provoking earthquake.

This research analyses the coseismic stress change and its postseismic response in the hot lower crust and upper mantle viscoelastic flow during the succession of the three major earthquakes (Mw ≥ 6.0) that occurred in the XVI-century in the EBSZ. The 13-year time window of this cascade suggests that the viscoelastic relaxation of the ductile lower crust, which typically occurs faster during the first one or two decades, may have significantly impacted its occurrence. In order to estimate the combined ΔCFS, the study requires earthquake source modeling and a good understanding of rheology, both of which pose difficulties in the EBSZ region. The subsequent sections provide a detailed explanation of the methods employed to address these challenges. The findings of this study strongly indicate the possibility of a stress-triggering connection between the three historical events and spotlight the importance of both coseismic and postseismic stress estimations in identifying earthquake linkage in the pre-instrumental period.

2. Geological Setting

2.1. General Tectonic Framework

The Betic Cordillera, along with the Alboran Sea and the Rif-Tell cordilleras in North Africa, conforms the westernmost extension of the Alpine Orogen. Since the late Miocene, compressive regional stress governs regional tectonics, with a NNW-SSE shortening that coexists with EW extensional tectonics in the Alboran Sea. In this sector, the 5–6 mm/yr NNW- SSE current convergence between Nubia and Eurasia tectonic plates (De Mets et al., 2015) distributes over a wide territory of complex tectonics conforming a diffuse contact showing a moderate seismic activity (Figure 1). A main tectonic feature controlling present-day deformation is the Trans Alboran-EBSZ, a prominent zone of strike-slip faulting, that separates the eastern and the western Alboran sectors (De Larouzière et al., 1988; Silva et al., 1993).

There are a variety of geodynamic models proposing different evolutionary scenarios of the Betic-Atlas-Rif system and the Alboran Basin, including those involving delamination of subducted continental mantle

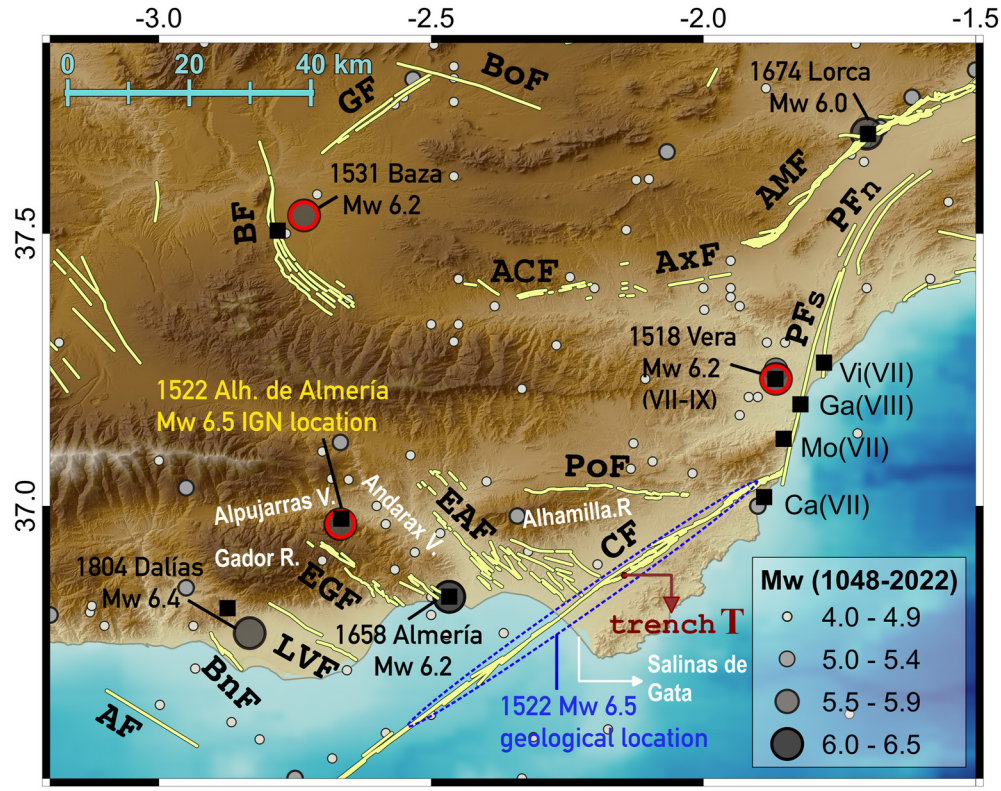

Figure 1. Seismotectonic and geographical context of the study area. The macroseismic epicenters of the XVI-century earthquake cascade (1518, 1522, and 1523) are outlined in red. Black squares situate the towns associated with the highest macroseismic effects related to these event. The location of towns affected by the 1518 Vera earthquake are indicated along with their estimated intensities (Silva et al., 2019) (Vi: Villarricos; Ga: Gafarillos; Mo: Mojacar; Ca: Carboneras). The 1522 Alhama de Almeria event was felt with EMS intensity VIII-IX in many villages along the Alpujarras and Andarax valleys, as well as in Almeria city. For this event the probable location of the epicenter along the carboneras fault trace on the base of geological evidence (e.g., Masana et al., 2018; Reicherter & Becker-Heidmann, 2009) is also indicated. Other three important events (Mw ≥ 6.0) later cited in the text are also identified in the figure. Lines depict Quaternary-active faults from Quaternary Active Faults Database of Iberia database (IGME, 2022) (AF:Adra Fault; AxF: Albox Fault; AMF: Alhama de Murcia Fault; ACF: Almanzora Corridor Fault; BnF: Balanegra Fault; BF: Baza Fault; BoF: Botardo Fault; CF: Carboneras Fault; EGF: East Gador Fault System; EAF: El Alquian Fault System; GF: Galera Fault; LVF: Loma del Viento—LLano del Águila Fault; PFn,s: Palomares Fault Northern and Southern sections; PoF: Polopos Fault). Earthquake catalog is declustered and homogenized to Mw (Cabañas et al., 2015; IGN & UPM, 2013).

lithosphere, rollback of the western Mediterranean subduction system and fragmentation and westward indentation of the Alboran domain (De la Peña et al., 2021; Diaz et al., 2021). The eastern Betic are subjected to the indentation of the Alboran Domain, in which kinematics and tectonic fabric are differentiated from the Iberian lithosphere (Palano et al., 2015; Tendero-Salmerón et al., 2022). The structure of the lithosphere in the eastern Betic is characterized by the presence of two contrasting types, namely the Iberian and the Alboran types, as has been evidenced in numerous geophysical studies (e.g., Banda & Ansorge, 1980; Banda et al., 1993; Carbonell et al., 1995; García-Dueñas et al., 1994). The Iberian type corresponds with the former Iberian plate continental passive margin, which was overthrusted in Miocene times by the Alboran microplate leading to the formation of the Betic orogen. The Iberian type corresponds to a well-structured three-layered continental crust, while the Alboran one is a two-layered crust undergoing progressive thinning and heat flux increment toward the Alboran Sea (Banda & Ansorge, 1980; De Lis Mancilla & Diaz, 2015; Fernàndez et al., 1998; García-Mayordomo, 2005; Torne et al., 2015) and eventually turning to oceanic crust in the south Balearic basin (Comas Minondo et al., 1995; Polyak et al., 1996; Poort et al., 2020). The role of a ductile lower crust in accommodating the differential deformation between the Iberian continental crust and the Alboran domain is relevant, as evidenced by the significant crustal thinning observed in seismic receiver function profiles (Morales et al., 2022) and in thermal modeling results (Torne et al., 2023). Accordingly, rheological studies in different regions of Betic Cordillera show that the thickness of the brittle and ductile portions of the lithosphere vary in a NW-SE as well as in ENE-WSW trend

(e.g., Fernández-Ibáñez & Soto, 2008; García-Mayordomo, 2005; Soto et al., 2008; Weijermars, 1987). Negredo et al. (2020) developed geodynamic models of the westernmost Mediterranean margin that included sensitivity tests to different rheological configurations, all of which contained a relatively low-viscosity layer at lower crustal levels. These studies clearly point to significant viscosity variations to explain the tectonics of the study area.

2.2. Seismicity and Active Faults

The study area is characterized by a moderate seismic activity. No earthquake with a magnitude of 7 or higher, or equivalent macroseismic intensity, has been recorded in the IGN (National Geographical Institute of Spain) earthquake catalog at shallow crustal levels. The first macroseismic assessment in this catalog dates back to 1048 AD, while archeoseismological evidence indicates earthquakes that occurred in the Neolithic and Roman periods (cf. Silva et al., 2019). Although the first bulletin of instrumentally recorded events dates to 1924, the current instrumental era did not officially begin until 1962 (cf. González, 2017). Since 1920, any crustal earthquake with epicenter in the study area has not exceeded a magnitude of Mw5.1.

Hence, the larger and more damaging events in the IGN catalog belong to the historical period, yielding difficulties in determining the precise magnitude and location of earthquakes because they are usually assigned to the regions with the most substantial damage based on the available information. Moreover, it is challenging to establish the specific active faults responsible for generating historical earthquakes due to considerable uncertainties, particularly when there is no univocal description in the chronicles of primary effects, such as a fault surface rupture. Considering the enormous anthropogenic modification of the territory in Southern Iberia, it is very unlikely that any such features would have survived until the present day. Fortunately, over the last few decades, numerous studies on active tectonics and paleoseismological research have been developed in the area (cf. Sanz de Galdeano et al., 2019). One significant outcome of these efforts is the development of the Quaternary Active Faults Database of Iberia (QAFI) (García-Mayordomo et al., 2012, 2017; IGME, 2022).

Quaternary-active faults in the Betic Cordillera are usually not longer than 30 km, striking NNW-SSE and NE-SW primarily to ENE-SSW, and slip rates generally lower than 0.5 mm/yr (García-Mayordomo et al., 2012, 2017; IGME, 2022). An important exception to this general frame is the EBSZ (De Larouzière et al., 1988; Silva et al., 1993) which extends in a sigmoidal shape along ca 500 km from the Alborán Sea to onshore Iberia and the Mediterranean (Figure 1). This crustal-depth fault system is composed of a number of faults of different geometries, trends, kinematics and slip rates, namely from SW to NE: Carboneras, Palomares, Alhama de Murcia, Los Tollos, Carrascoy, and Bajo Segura. The most active faults of this system are the NE-SW 140 km long left-lateral strike-slip Carboneras fault, and the NE-SW 87 km long left-reverse dip-slip Alhama de Murcia Fault, with average slip rates of 1.3 and 1.6 mm/yr, respectively (Gómez-Novell et al., 2022; Martínez Díaz, Bejar-Pizarro, et al., 2012; Martínez Díaz, Masana, & Ortuño, 2012; Moreno, 2010; Moreno et al., 2015). Bridging the 60 km gap that separates both faults there is the NNE-SSW left-lateral strike-slip Palomares fault, with a contrasting slip rate of 0.2 mm/yr (Gómez-Novell, 2021). The Baza Fault is another crucial tectonic feature in the study area (Alfaro et al., 2008). This NNW-SSE to NW-SE normal fault lies in the central part of the cordillera disconnected from the EBSZ, controlling the western margin of the so-called Baza basin formed in Neogene times (Sanz de Galdeano & Vera, 1992). The Baza fault has also been the motive of paleoseismological studies demonstrating its seismogenic character and constraining an average slip rate of 0.45 mm/yr (Medina-Cascales et al., 2020).

Apart from the EBSZ faults, there are other faults and fault systems relevant for the purpose of this study (Figure 1). West of Carboneras Fault, there is the 36 km long El Alquián normal faults system, a wide NW-SE fault zone (5–10 km) controlling the termination of the Alhamilla Range, Andarax valley and the coastline. To the west of the El Alquián system, there is the East Gador normal fault system (ca 5 km wide), also striking NW-SE, cutting across the Gador Range for ca 20 km until dipping in the sea (Pedrera, 2012). Finally ca 60 km north of the Almeria area, in the Baza basin, there is the Galera fault (Medina-Cascales, 2021; Medina-Cascales et al., 2021). This feature locates ca 10 km east of the Northern tip of the Baza fault striking nearly perpendicular to it. The Galera fault is a left-lateral reverse fault that extends NE-SW for ca 30 km. Paleoseismological research on the fault has found evidence of 3–7 events since 24,000 BCE (Medina-Cascales, 2021; Medina-Cascales et al., 2021).

2.3. The XVI-Century Earthquake Cascade

The 1518 Vera Earthquake: The 9 November 1518 earthquake (I_{EMS} = VIII-IX; I_{ESI} = IX) known as the Vera event, completely destroyed the ancient town of Vera (Almeria) and heavily damaged other towns and constructions

(e.g., Villaricos, Garrucha, Mojacar, Carboneras) along the conspicuous NNW-SSE ca 30 km coastline controlled by the Palomares fault (cf. Martınez-Solares & Mezcua, 2002; Silva et al., 2019) (Figure 1). The scarce historical documentation is heavily focused on describing the damage to the constructions and casualties. As a result, no evidence has been found to support the occurrence of any environmental effects that could be attributed to a surface fault rupture. The macroseismic epicenter of the earthquake is located at the site of the ancient Vera town, which was founded on top of a very narrow and prominent hill, indicating a possible concurrence of ground motion amplification (topographic effect) (Silva & Roquero, 2017). Nevertheless, the Vera event is very likely related to the Palomares fault based on the damage distribution along the coast and also because it is the only Quaternary-active fault in the area potentially capable of producing major events (Mw $\geq$ 6.0) (IGME, 2022). The magnitude of the Vera earthquake can be approximated with average of Mw6.2 using the Cabañas et al. (2015) moment magnitude on EMS intensity relationships produced in the frame of the commission for the official Spanish Hazard Map (IGN & UPM, 2013). The used magnitude for the Vera earthquake in this study is Mw6.2.

The 1522 Alhama de Almeria Earthquake: Less than 4 years after the Vera event, another major earthquake took place in the area on 22 September 1522 (I_{EMS} = VIII-IX; I_{ESI} = IX). This earthquake was felt to a wider extent than the Vera event. It caused severe damage in the city of Almeria on the coast and in many other towns located along the Andarax River and Alpujarras valleys (Figure 1), adding up to more than 1,000 fatalities. The estimated average magnitude of the event is quoted in the IGN catalog as Mw6.5 after Mezcua et al. (2004) (IGN & UPM, 2013).

Interestingly, there is a written record of sea anomalies in Almeria city as well as on the African coast that have been interpreted as tsunami effects (Huerta & Silva, 2014). To the west of Almeria city, in Salinas de Cabo de Gata, where the Carboneras fault comes into the sea, shallow drilling has identified tsunami deposits in cores being the most recent dated coeval with the 1522 earthquake (Reicherter & Becker-Heidmann, 2009). These authors suggest the strike-slip Carboneras fault (Masana et al., 2018; Moreno et al., 2015) as the source of the 1522 event, likely triggering submarine landslide that eventually generated the tsunami. However, recent modeling of the Carboneras fault shows its potential for producing noticeable tsunamis, locally damaging, despite its near pure strike-slip kinematics (Álvarez-Gómez et al., 2022).

The IGN catalog (Martınez-Solares & Mezcua, 2002) locates the macroseismic epicenter of the event on the steep slopes of the Gador Range, at approximately a middle distance between the most affected towns located in the Andarax and Alpujarras valleys, ca 24 km NW inland from Almeria city (Figure 1). Accordingly, some authors suggest the Eastern Gador Range Fault System as a possible source for the 1522 event (e.g., Pedrera, 2012). Nevertheless, the reason that most of the historical damage descriptions are from villages far from the Carboneras fault zone can be explained due to the fact that this territory was poorly inhabited at that time compared to the Andarax and Alpujarras valleys. Additionally, topographical site effects might well impact the villages on the scarps slopes of those valleys in addition to widespread landslides phenomena (Huerta & Silva, 2014).

The Carboneras fault has been the subject of active tectonics research both onshore and offshore, evidencing its Holocene activity (López-Escudero et al., 2019; Masana et al., 2018; Moreno et al., 2015; Reicherter & Hübscher, 2007). Paleoseismological research has been able to infer a number of paleo-earthquakes attributed to the fault. The most recent one was observed at trench T (Figures 1 and 6), offsetting 3.8 m a channel dated coherently with the 1522 event; indicating a potential magnitude for the event around Mw7.0–7.2 and a 46–58 km surface rupture length (López-Escudero et al., 2018, 2019). Therefore in this study a range of magnitude (Mw6.5–7.1) is applied for modeling this event.

The 1531 Baza Earthquake: Almost 9 years after the 1522 event, on 30 September 1531, a strong earthquake occurred in the Granada Province. It caused ~400 deaths and practically destroyed the town of Baza, located ca 90 km far from the Palomares and Carboneras faults. The town of Baza is sited right on the Baza Fault zone, which controls the western border of the Baza intermontane Neogene basin (Alfaro et al., 2008). Even though there is no written description of a fault surface rupture there is general agreement that the Baza fault was responsible for the 1531 event (cf. García-Tortosa & Silva, 2017). Its estimated magnitude has an average of Mw6.2 (Cabañas et al., 2015; IGN & UPM, 2013) which is the used magnitude in this study. Recent paleoseismological work has evidenced the occurrence of at least seven paleoevents since 45,378 BCE (Medina-Cascales, 2021; Medina-Cascales et al., 2020).

The Baza fault shows two distinct sections, the town of Baza is located approximately in the middle. The Northern section strikes NNW-SSE for ca 20 km bounding with the neighboring Guadix basin, while the Southern

Table 1
Data Considered for Modeling the Occurrence of the Three XVI-Century Events (1518, 1522, and 1531) on Their Respective Causative Faults (Palomares, Carboneras, and Baza)

		Source fault		
Event date	Magnitude (M_w)	Name	Strike/dip/rake	$L \times W$ (km^2)
9 November 1518	6.2	Palomares	14°/90°/10°	45 × 8
22 September 1522	6-5-7.1	Carboneras	48°/90°/10°	110 × 11
30 September 1531	6.2	Baza	341°[a]/65°/−90°	38 × 12

[a]Average value for a curved trace striking between 315° at SE and 370° at NW.

section extends NW-SE for ca 15 km, controlling the border with the Baza Range and conforming a 5–7 km wide fault zone in which 13 different strands have been recognized (Medina-Cascales, 2021).

3. Data and Methodology

When an earthquake occurs, the two sides of a fault plane slide past each other, resulting in the emergence of an altered deformation field. This coseismic deformation leads to a perturbation in the crustal stress field that can modify the effective stresses on active faults, and cause advancing or delaying their rupture (Harris, 1998; King & Cocco, 2001; Stein, 1999). Additionally, because the lithospheric layers (i.e., lower crust and upper mantle) have lower viscosity, the yield coseismic stress changes in the elastic upper crust induce postseismic viscoelastic relaxation in these layers. This process can either enhance or mitigate the coseismic built-up stress and alter the stress-triggering effect over time (Burgmann & Dresen, 2008; Pollitz & Sacks, 1995, 1997). This time-dependent process is modeled applying the following steps, from the day of the 1518 Vera earthquake and implying the three events with data as given in Table 1. The average kinematics and geometry of the faults are adopted from QAFI database (IGME, 2022).

1. Configuration of the mechanical model of the lithosphere, with the specification of the thicknesses and rheological properties of each layer.
2. Configuration of a source rupture model representing the historic earthquake, consistent with generating-fault geometry earthquake magnitude.
3. Computation of coseismic and postseismic deformation field resulting from the rupture described in step 2.
4. Analysis of combined (coseismic + postseismic) ΔCFS for the average strike/dip/rake of selected target fault to evaluate whether there is stress-mediated interaction between distinct earthquakes over time, as subsequent earthquakes contribute to cumulative combined ΔCFS.

This study does not include the ΔCFS because of inter-seismic processes.

3.1. Configuration of the Lithosphere

The lithosphere model used in this work (Table 2) is defined based on a combination of the so-called Cartagena and Almería crustal blocks as defined in García-Mayordomo (2005). This two-layered crustal model represents the thinning and heat flux increment that the Alboran-type lithosphere experiences toward the Alboran Sea and the transition to an increasingly mafic lower crust in the Cartagena block. Rheological modeling indicates brittle

Table 2
Rheological Parameters Considered for the Six Tested Lithospheric Models

					η (Pa s) for model					
	Thickness (km)	V_p (km/s)	V_s (km/s)	ρ (kg/m^3)	m_1	m_2	m_3	m_4	m_5	m_6
Upper crust	12	6.00	3.46	2,700	Elastic ($\eta \to \infty$)					
Lower crust	11	6.90	3.87	2,900	10^{18}	10^{18}	10^{18}	10^{19}	10^{19}	10^{20}
Upper mantle	49	8.20	4.60	3,200	10^{19}	10^{20}	10^{21}	10^{20}	10^{21}	10^{21}

deformation in the upper crust until 8 km depth and again at the interface with the lower crust at 12 km depth, coincidentally with the 90% percentile of the seismic hypocenters distribution. Considering these observations, a representative average seismogenic depth of 10 km is selected for the calculations. The mechanical thickness of the lithosphere, that is, the depth at which the supported deviatoric stress drops below 1 MPa (Ranalli, 1995), is estimated at 72 km depth (García-Mayordomo, 2005).

In general, at stress levels that are sufficiently low to induce a rupture in preexisting fractures on faults, the typical rheological profile of an active continental lithosphere can be described by the "jelly sandwich" model (Burov, 2011). This model is characterized by a weak mid-to-lower crust subjected to higher pressures and temperatures that involve both elastic and viscous deformation and a strong mantle composed dominantly of dry olivine (Burgmann & Dresen, 2008; Hirth & Kohlstedf, 2003). The limited information about the magnitude of viscosity η, for lithospheric layers beneath the EBZS makes it difficult to establish specific values for it. Weijermars (1987) study on the Palomares shear zone results in a softened upper crust viscosity of order 10^{20} Pa s in the zone versus 10^{25} Pa s outside and at the boundaries of Palomares shear zone. Negredo et al. (2020) modeling the westernmost Mediterranean margin geodynamics, assume a constant composite (for visco-plastic rheology) viscosity of the same order for the upper crust and a viscosity of 2×10^{19} Pa s for a weak lower crust. For the lithospheric mantle, their approach suggests a moderate viscosity of order 5×10^{22} Pa s. Tesauro et al. (2011) analyze the shear strain rate in the European lithosphere and using their result for a soft rheology model in the area of this study and an assumption of 100 MPa for the deviatoric shear stress in the lithosphere (Turcotte & Schubert, 2002) the corresponding viscosity would be between 10^{17} and 10^{21} Pa s.

The range of suggested viscosity values implies testing a combination of values that could be associated with the study zone. Accordingly, three orders of magnitude viscosity parameters $\eta = 1 \times 10^{20}$, 10^{19} and 10^{18} Pa s are considered for simulating a lower crust with low, medium, and high ductile properties, respectively. Likewise, three orders of magnitude are considered for the upper mantle viscosity, keeping the lower crust with lower viscosity in each model. The resultant combination presents six models as in Table 2 where model m_3, with a low viscosity for the lower crust, is used as the reference model. This choice is made based on similar studies (e.g., Mohammadi, 2022; Verdecchia et al., 2018). Moreover, it allows for a better examination of the short-term viscoelastic relaxation effect in the lithosphere compared to other models (Section 4). For modeling the viscoelastic behavior, the Maxwell body equation, a commonly used viscoelastic behavior that suits the large tectonic strains (e.g., Freed et al., 2006; Liu et al., 2022; Verdecchia et al., 2018), is applied. After an immediate elastic response, Maxwell materials relax exponentially (Burgmann & Dresen, 2008) and their linear strain-rate $\dot{\varepsilon}$ is consist of two contributions, a viscous and an elastic response: $\frac{\dot{\sigma}}{G}$ and $\frac{\sigma}{\eta}$, where $\dot{\sigma}$ stands for the stress rate and G is the shear modulus. A typically used value of 0.25 for the Poisson ratio (Stacey & Davis, 1977) and a shear modulus of 32 GPa are considered for the upper crust.

3.2. Source Modeling

Modeling the source of historical earthquakes is challenging. The documented information available is mainly qualitative. As a result, estimating the location of the epicenter and the distribution of slip on the causative faults necessarily involves certain simplifications, particularly if no modern earthquake rupture record and its corresponding source model exist for such a fault.

The applied approach in this study first uses the empirical relation $\log M_0 = 16.05 + 1.5$ Mw, by Hanks and Kanamori (1979), to find the seismic moment, and then uses $M_0 = G$ A $\bar{S}$, by Aki (1966), to get an estimation of A $\bar{S}$ product, where $\bar{S}$ is the average slip amount over a ruptured area of size A, and G is the shear modulus in the upper crust, here taken as 32 GPa. The next step is to distribute the slip amount over the causative rupture plane of average size A. The fault plane is then divided into smaller patches of the same size. In order to achieve a smoother slip distribution, a relatively small patch size of 1 km^2 is utilized. The study also takes into account the empirical relations established by Wells and Coppersmith (1994) between various parameters, such as rupture geometry (e.g., area, width, surface length, subsurface length) and slip amounts (e.g., surface slip, maximum surface slip, subsurface slip), and earthquake moment magnitude, ensuring their consistency. To account for the lack of detailed information on the hypocenter, maximum slip, or centroid locations, a 2D ellipsoidal distribution with smoothed tapers on the edges is used to distribute the slip over constructed patches (e.g., Yazdi, 2019). This simple distribution results in a nearly constant stress drop within the rupture area (Santoyo et al., 2005), assuming

strike-wise symmetry. However, a slight dip-wise asymmetry is applied to place the maximum slip closer to the seismogenic depth of 10 km in this study. For all three events analyzed in this work, the modeled ruptured area does not cover the entire fault plane. Therefore, shifting the estimated ruptured plane of average size A along the strike and/or dip and within the fault boundaries allows for multiple plausible models for each event. However, additional constraints, such as paleoseismic research results (i.e., Section 2.3), can reduce the extent of shifting possibilities.

Given the relatively small width (~8–11 km) of the causative faults in this study, the modeled ruptured areas representing the three earthquakes would only be shifted along their fault strike. As it is explained in Section 2.3, the 1518 Vera earthquake almost certainly ruptured the southern section of the Palomares fault. Therefore, its modeled ruptured area, assuming an average magnitude Mw6.2, is located at the southernmost end of this fault (Figure 6). However, more than one likely scenario exists for the 1522 Alhama de Almeria earthquake on the >100 km long Carboneras fault. Not only do multiple estimations exist for its average magnitude (Section 2.3), but also shifting its ruptured area from NE to SW implies more scenarios. However, the constraints arising from paleoseismic studies mentioned in Section 2.3 (i.e., results from trench **T** in Figure 1 and evidence of tsunami) somehow limit the possible options. Accordingly, a slip distribution model with considerable rupture onshore at the location of trench **T** can better simulate this event. Although the coastal landslide accompanied by strike-slip faulting (Hornbach et al., 2010) can also cause tsunami, the dip-slip component of the Carboneras fault endows it with a genuine capacity to generate a locally damaging tsunami (Álvarez-Gómez et al., 2022). This suggests that a potential second constraint would be shifting the ruptured plane toward offshore. Figure 3a shows a 2D illustration of the shifted rupture area with a slip distribution that simulated a magnitude of Mw6.9 over the Carboneras fault. One of the examples in this figure (model No. 2) is also shown in 3D in Figure 6. Regarding the Baza earthquake, which is associated with a curved Baza fault, two different rupture scenarios are proposed. In one scenario, the Northern section of the fault ruptures with a strike of 355°, while in the other scenario, the Southern section ruptures with a strike of 315°. The simulation of Mw6.2 for the northern rupture scenario is illustrated in Figure 6.

3.3. Coseismic and Postseismic Stress Changes

In this study, a three-layered viscoelastic half-space modeling approach is used to estimate the spatial and temporal distribution of cumulative coseismic and postseismic stress changes following the 1518 Vera earthquake at a seismogenic depth of 10 km. The program PSGRN/PSCMP by Wang et al. (2006) is employed for this purpose. Table 2 provides the rheological parameters used in the modeling. The resulting stress changes may alter the pre-existing static ΔCFS over nearby fault planes (target faults), potentially pushing them toward failure. To estimate the due $\Delta CFS = \Delta\tau + \mu^*(\Delta\sigma_n)$ for the shear stress change $\Delta\tau$ consistent with the slip direction of the target faults (IGME, 2022), two effective frictions μ^* of 0.4 and 0.6 are taken into account. The $\Delta\sigma_n$ is the change in the normal stress and positive for tension.

4. Results

4.1. The Effect of 1518 Event

The combined ΔCFS triggering influence of the 1518 Vera earthquake could have driven the Carboneras fault closer to rupture in 1522 (Figure 2a). The coseismic ΔCFS amount with magnitude considered within an earthquake-triggering context, yet does not involve further than 5 km of the Carboneras northernmost end. Though, in less than 4 years, the lithospheric viscoelastic relaxation increases ΔCFS up to 0.4 bars. The spatial extension of this postseismic stress-triggering effect spans to the southwest, particularly at higher depths. Accordingly, a combined $\Delta CFS \geq 0.2$ bars implicates about 25 km of the Carboneras northernmost end (Figure 2b).

The triggering effect of the 1518 Vera earthquake on the state of stress over the Baza fault, despite being positive, does not have a considerable magnitude. The combined ΔCFS remains less than 0.05 bars even after a period of approximately 13 years, up to 1531. However, the cumulative effect of the second event in the cascade, the 1522 Alhama de Almería earthquake, is yet to be added in order to better understand the occurrence of the 1531 Baza earthquake.

4.2. The Effect of the 1518 and 1522 Events

Following the 1522 earthquake on the Carboneras fault, the cumulative combined ΔCFS significantly impact the Baza fault, although not immediately. Over the next 9 years, the viscoelastic relaxation causes the stress-triggering to evolve toward this fault (Figure 3b).

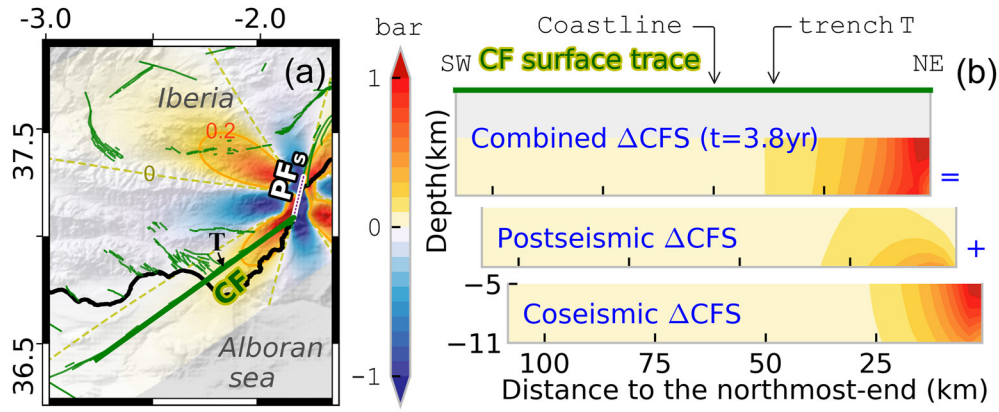

Figure 2. The combined (coseismic + postseismic) ΔCFS because of the 1518 earthquake solved for Carboneras kinematics, (a) at a depth of 10 km after almost 4 years, and (b) between depth of 5 and 11 km over Carboneras fault plane.

As previously explained in Section 3.2, simulating the 1522 event implies trying multiple scenarios about the length and location of its ruptured area on the Carboneras fault. Figure 3a shows an example of the 2D smoothed ellipsoidal slip distribution that models rupture of a Mw6.9 over the Carboneras fault and its gradual shifting from the NE to the SW. The more proper shift should be the one that results in a considerable surface rupture close to the location of trench **T** (see Figure 1) at a ~35 km distance from the northernmost end of the Carboneras fault. For instance, among five models the model No. 2, 3, and 4 satisfies this constraint best. Applying the model No. 3 (with epicenter on ~40 km from the NE-end of the Carboneras), the 0.2 bar isolines in Figure 3b display how the cumulative stress-triggering effect over the Northern section of the Baza fault increases after the 1522 earthquake on the Carboneras fault. Consequently, the postseismic process of lithosphere viscoelastic relaxation could have contributed to the occurrence of the 1531 Baza earthquake.

However, the extent of the ΔCFS increment, is potentially sensitive to the varying strike of the Baza fault along its curved shape and the magnitude and location of the Carboneras earthquake, among other factors. With only one used magnitude for the 1518 Vera earthquake (Mw6.2), the cumulative combined ΔCFS is estimated for a range of magnitudes (Mw6.5–7.1) for the 1522 Alhama de Almeria earthquake; for each assumed magnitude, the spatial effect of moving the maximum slip location on yield ΔCFS is also considered.

Figure 4 displays which section is more prone to positive ΔCFS and through different scenarios also illustrates the circumstances that are more likely to result in stress-triggering of the 1531 Baza earthquake. Each

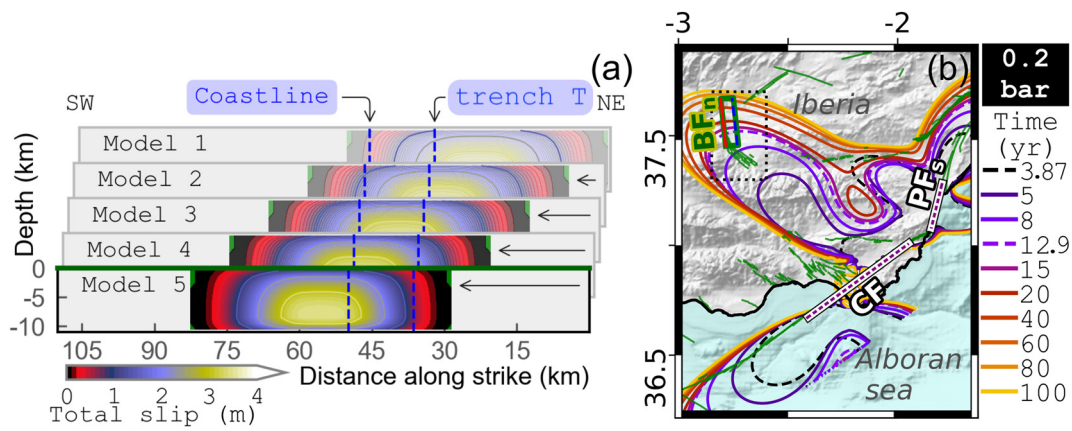

Figure 3. (a) Five different rupture models of a Mw6.9 earthquake by the Carboneras Fault. Models results from considering the rupture area shifting along the trace of the fault and constrained by the coastline and location of paleoseismic trench **T**. (b) Time variation of cumulative combined ΔCFS because of model No. 3 on Northern Baza fault (BFn) 355°/65°/−90° at a depth of 10 km. Colored 0.2 bar isolines scale with time. Rupture sections of the Palomares (PFs) and Carboneras faults (CF) are also shown (b).

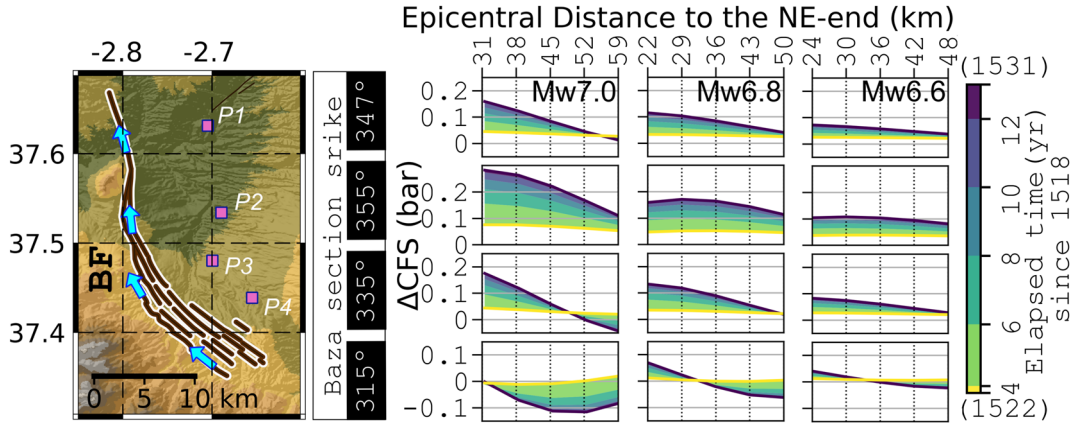

Figure 4. The temporal variation of cumulative combined (coseismic + postseismic) ΔCFS because of 1518 Vera Mw6.2 and the 1522 Alhama de Almeria events at four different sites (*P1* to *P4*) associated with trends of the Baza fault (blue arrows: 347°, 355°, 335°, and 315°) at 10 km depth. The shown result is for three different Mw values (7.0, 6.8, and 6.6) of the 1522 event and a combination of five different rupture area placements (similar to Figure 3a) for each magnitude. The five rupture placements of each magnitude are indicated by the distance from maximum slip locations to the NE-end of the Carboneras fault.

row of panels in Figure 4 addresses the sensitivity of ΔCFS to the target fault strike and remarks a substantial stress-triggering influence on the Northern section, which also appears as the most controlling kinematics of the Baza fault (cf., Alfaro et al., 2021). The triggering effect of ΔCFS decreases as the striking angle changes from NS to NW-SE and ultimately becomes negative for the Southern section of the fault. This strike-dependent result remains consistent for variation of dip and rake (dextral or sinistral components) within the uncertainty range given by Medina-Cascales et al. (2020) (see Figure S1 in Supporting Information S1). The columns of panel in Figure 4 reveals how the size of ΔCFS directly depends on the assumed magnitude for the 1522 events. Assuming a magnitude of Mw6.6 for the 1522 event, the estimated cumulative ΔCFS is close to 0.1 bar. As the magnitude used in the calculation increases, the estimated ΔCFS also increases to approximately 0.2 bar for a Mw6.8 and approaches ~0.3 bar for a Mw7.0. However, as mentioned previously, the ΔCFS still fails to explain the stress-triggering hypothesis for the Southern section of the Baza fault.

In general, the ΔCFS is always positive for points *P1* and *P2*, representative of the Northern section of the Baza Fault. For the Southern section (*P3* to *P4*) the sign of ΔCFS is more dependent to the location of rupture on the Carboneras, particularly at the southernmost point (*P4*).

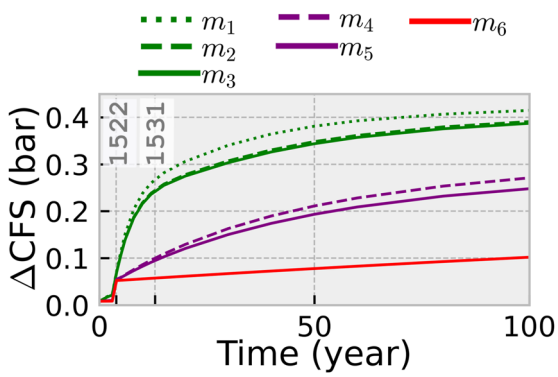

Figure 5. Hundred years variation of cumulative combined (coseismic + postseismic) ΔCFS for the six different rheological models detailed in Table 2 (Section 3.1). Calculations are performed for the Baza Fault at site *P2* (355°/65°/−90°; see Figure 4) after a Mw6.2 earthquake on the Palomares fault followed by a Mw6.9 earthquake on the Carboneras fault (as in Model No. 2 in Figure 3a) in less than 4 years.

Both size and rate of ΔCFS, however, are sensitive to the applied rheology model (Table 2). Figure 5 compares the cumulative combined ΔCFS applying each model in Table 2 for the first hundred years. All models present decaying rates in the yield stress changes. Given the small impact of parameter μ^* on the pattern of stress distribution (King et al., 1994) a more conservative value of 0.4 is used for interpreting the results presented in this section. Figure S2 in Supporting Information S1 shows a similar behavior of ΔCSF curves for $\mu^* = 0.6$, where a slightly greater (in |ΔCFS| size) stress-triggering effect can be seen. For a less viscous lower crust (e.g., $\eta = 10^{18}$ Pa s in models m_1 to m_3), the postseismic relaxation effect is more important in the first ~15 years. Whereas, in the short-term, the significance of viscoelastic relaxation is minimal when the lower crust and lithospheric mantle exhibit high viscosity values (e.g., model m_6).

5. Discussion

Examining the induced stress-triggering state following the XVI-century cascade can provide insight into how this cascade may have contributed to the stress increase over the nearby faults after 1531. Further important

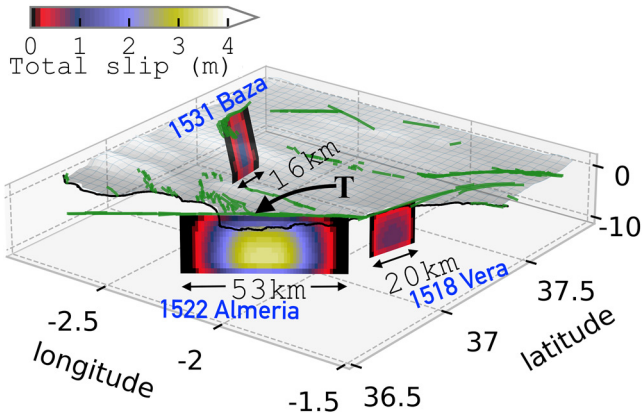

Figure 6. Fault ruptures model considered to study the impact of the XVI-century earthquake cascade in nearby Quaternary-active faults (see Figure 7). For the 1518 Vera, 1522 Alhama de Almeria, and 1531 Baza events, a Mw of 6.2, 6.9, and 6.2 corresponding to a rupture of 158, 575, and 194 km^2 on the Palomares fault Southern section, Carboneras fault as model No. 2 in Figure 3a, and Baza fault Northern section, respectively, have been considered for the calculations.

crustal earthquakes with Mw ≥ 6.0 in the proximity of this cascade are the 1658 Almeria Mw6.2, the 1674 Lorca Mw6.0, and 1804 Dalias Mw6.4 (Cabañas et al., 2015; IGN & UPM, 2013; Mezcua et al., 2004). The responsible faults identified for the last two events are the Alhama de Murcia fault (Martínez-Díaz et al., 2019) and the Loma del Viento—Llano del Aguila fault (De Pro-Díaz et al., 2023; Molins-Vigatà et al., 2022; Murphy, 2019). However, for the 1658 Almeria event, there is no clear relation with any particular fault. It could have been the Carboneras, the Polopos, or any of the NW-SE normal fault systems common in the area, namely the El Alquian or East Gador fault systems (Figure 1). Accordingly, applying the results described in Section 4.2, the source model of the Baza earthquake is added to the scenario and placed over a strike of 355° to model the cumulative combined deformation following all three events. The same mechanical-rheological parameters and source models of the 1518 and 1522 events used before are applied.

Figure 6 shows a scenario consisting of the southern section of Palomares, the northern parts of Carboneras, and the northern section of the Baza fault rupturing in 1518 with Mw6.2, 1522 with Mw6.9, and 1531 with Mw6.2, respectively, for which the cumulative combined ΔCFS is estimated for all potentially target Quaternary-active faults in the studied area (Figure 7). The assessment is carried out for Alhama de Murcia (Goñar-Lorca and Lorca-Totana sections), Galera, Botardo, Carboneras, Palomares (both Southern and Northern sections), Almanzora Corridor, Albox, Polopos (both Eastern and Western sections), El Alquian, East Gador, Loma del Viento, Balanegra, and Adra faults (see Figure 1), using a depth range from 6 to 10 km and a time frame of up to 140 years when the 1658 Almeria Mw6.2 earthquake occurred. Fault mechanisms are taken from the QAFI database (IGME, 2022) and are listed in Table S1 in Supporting Information S1.

The stress buildup along the outward extensions of the rupture areas of three source faults is evident in the ΔCFS maps shown in Figure 7. Of particular note is the significant increase in positive ΔCFS along the Palomares fault, which is remarkable given that the earthquake record along the fault zone since the 1518 Vera event only comprises low-magnitude events (Mw < 5.0). This situation suggests that the Palomares fault has been accumulating substantial stress since 1518. However, this fault has been recognized as a significant contributor to epistemic uncertainty in probabilistic seismic hazard studies conducted in the EBSZ (Gómez-Novell, 2021) due to the lack of paleoseismological research and a robust slip rate estimation for the upper Pleistocene, unlike the other faults that formed the EBSZ. Hence, the obtained results highlight the importance of studying the Palomares fault's recent activity for future seismic hazard assessments in the region.

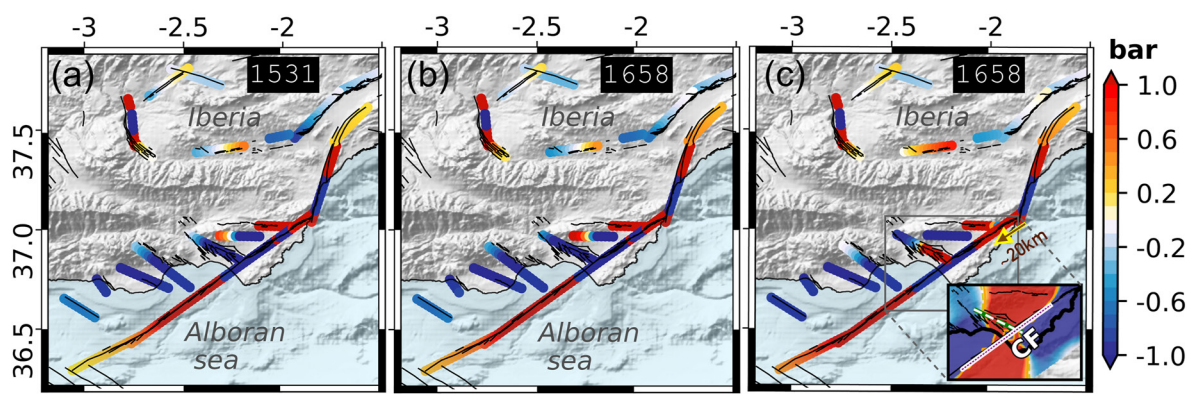

Figure 7. The cumulative combined ΔCFS solved for each fault, with geometry and rake provided by IGME (2022), at a depth of 6 km, and because of a rupture scenario as in Figure 6 for the XVI-century cascade (a) right after the 1531 Baza earthquake, (b) after 140 years since the 1518 Vera earthquake, and (c) when the 1522 Mw6.9 epicenter is shifted more to the southwest (as in model No. 4 in Figure 3a). The small window represents the result using the receiver fault geometry of the El Alquian fault; 121°/60°/−90°.

Potential stress-triggering effects are also observed over parts of the Polopos, Almanzora Corridor, and Galera faults (Figure 7a), and as time passes, the ΔCFS distribution and intensity vary slightly (Figure 7b). The triggering effects get larger when using a model (such as the model No. 4 in Figure 3a), in which the rupture area of the 1522 event is shifted more to the southwest (Figure 7c). It is noteworthy to mention that in 1964 there was a damaging earthquake (I_{EMS} = VII, Mw4.9) in the area attributed to the Galera fault (García-Tortosa et al., 2007).

Either section of the Alhama de Murcia fault clearly experiences insignificant or negative ΔCFS, suggesting that the 1674 Lorca event can not be connected to the XVI-century cascade (Figure 7). Similarly, it seems that the yield ΔCFS on the El Alquian, East Gador, Loma del Viento, Balanegra, and Adra faults creates a significant delaying effect. This implies that the XVI-century cascade might not have triggered subsequent major earthquakes over these faults (e.g., the 1658 and 1804 events). The ΔCFS maps for depths of 8 and 10 km are provided in Figure S3 in Supporting Information S1. Nevertheless, it is important to note that the results obtained for the El Alquian system are very sensitive to the epicenter location of the 1522 event along the Carboneras fault. Supposing the applied model has the epicenter of the 1522 event closer to the coast (as model No. 4 in Figure 3a), then the southeastern end of the El Alquian fault experiences a substantial stress buildup, mainly due to the coseismic impact of the 1522 event and its intensification during the postseismic period (Figure 7c). Therefore, it is not possible to thoroughly discard the hypothesis that the 1658 event may have occurred on the El Alquian system due to the stress-triggering impact of the cascade. There is no historical description of a proper tsunami related to this event but anomalous sea waves. However, the magnitude of the event was not large enough to generate a tsunami, and hence, an offshore section of the Carboneras fault that appears clearly charged could also be a source candidate for the 1658 event (Silva, 2017). Additionally, the Polopos fault in Figure 7 appears loaded too, and neither cannot be ruled out as a source for the 1658 Alemria earthquake. Figure S4 in Supporting Information S1 shows auxiliary ΔCFS maps solved for the candidate causative faults of this event. This result suggests that the three faults (El Alquian, Carboneras, and Polopos) remain as a possible source of this earthquake.

The discussed results are obtained under the assumption of rheology model m_3 (Table 2) and applying $\mu^* = 0.4$, and since the study method relies on modeling the ΔCFS, it is essential to note that there are inherent uncertainties associated with selecting physical parameters and rheological settings of the lithosphere. The ΔCFS distribution pattern is not considerably affected by the selection of the friction coefficient μ^*, which mainly controls the normal stress change. However, applying $\mu^* = 0.6$ enhances the magnitude of |ΔCFS|, maintaining consistency with the suggested results (see Figure S2 in Supporting Information S1). On the other hand, the choice of rheological model, particularly the viscosity of the lower crust, controls the development of the postseismic effect. One order of magnitude higher viscosity values (10^{19} Pa s) for this layer leads to a minor |ΔCFS|, yet the postseismic stress-triggering impact can not be ignored. Conclusion delivered in this study also involves simplifying assumptions such as the use of a three-layered lithospheric structure with 2D-homogeneity, application of average fault kinematic driven from geological data, and regular smoothed slip distribution for source rupture modeling. Further uncertainties that arise from such simplifications, specifically regarding the distribution of slip and its direction over the fault planes, however, are due to the inherent limitations associated with historical earthquake modeling and the slow tectonic deformation characteristic of the study zone.

6. Conclusions

This study provides insight into the potential mechanism that explains the occurrence of three major earthquakes (Mw ≥ 6.0) in the Betic Cordillera (Southern Iberia) during the early XVI-century. The results suggest that the stress transfer caused by viscoelastic relaxation could have played a key role in connecting these events, which occurred within a short time frame of just 13 years and were associated with different active faults. It is also proposed that the section of the Baza fault that ruptured in 1531 was the Northern NNW-SSE strike.

Further examination of coseismic and postseismic stress-triggering over an extended time period uncovers the potential impact of this cascade on nearby active faults in the study zone. Accordingly no evidence to support that the XVI-century cascade influenced the occurrence of the 1674 Lorca (Mw6.0) or 1804 Dalias (Mw6.4) events has been found, as their respective causative faults experience negative ΔCFS. Conversely, the 1658 Almería (Mw6.2) event could have been related to either the El Alquian system, Polopos fault, or an offshore section of the Carboneras fault, all of which undergone positive ΔCFS during the following 140 years.

Finally, the integration of historic and paleoseismic data with stress transfer modeling presented in this study delivers a feasible mechanism that connects earthquakes with different seismogenic sources separated in time

(years to decades) and space (tens of km). This approach, particularly in zones with active faults of low-stress accumulation and long interseismic periods, challenge the commonly assumed notion in the standard probabilistic seismic hazard assessments that seismic activity follows a Poissonian process, particularly for moderate to high magnitudes. The earthquake recurrence models in regions with slow tectonic deformation typically encounter challenges due to the lack or unavailability of data. Indeed, findings such as this study provide constraints for characterizing recurrence models applicable to faults capable of generating moderate-to-high magnitude events and coseismic and postseismic stress changes should be incorporated in future endeavors for fault-based and time-dependent seismic hazard assessment in the EBSZ.

Data Availability Statement

The earthquake data in this manuscript was adopted from the Database of Iberian Seismogenic Zones (IGME, 2015), accessible from https://info.igme.es/zesis and the National Geographic Institute (IGN, 2022), accessible from https://doi.org/10.7419/162.03.2022. The Quaternary Active Fault Database of Iberia (IGME, 2022), available at https://info.igme.es/qafi was used for the faults data. The PSCMP/PSGRN code (Wang, 2006) for calculating the coseismic and postseismic deformation can be accessed through https://git.pyrocko.org/pyrocko/fomosto-psgrn-pscmp. Figures were created with Matplotlib version 3.5.1 (Hunter, 2007) and the free and open source QGIS software version 3.18.3 (QGIS Development Team, 2021) which are accessible from https://matplotlib.org and https://www.qgis.org, respectively.

Acknowledgments
This research has the financial support of Project NSources, Grant PID2020-119772RB-I00 funded by MCIN/AEI/ 10.13039/501100011033. It was conducted in the frame of the postdoctoral Margarita Salas Fellowship program of Pouye Yazdi at Universidad Politécnica de Madrid, funded by the Spanish Ministry of Universities. PY carried out the study during her visiting period at Instituto Geologico y Minero de España (CSIC), which is also acknowledged. The authors want to thank the anonymous reviewers for their comments and suggestions that contributed to improve this paper.

References

Aki, K. (1966). Generation and propagation of G waves from the Niigata earthquake of June 16, 1964. Part 1. A statistical analysis. *Bulletin of the Earthquake Research Institute*, *44*, 23–72.

Alfaro, P., Delgado, J., Sanz de Galdeano, C., Galindo-Zaldívar, J., García-Tortosa, F. J., López-Garrido, A., et al. (2008). The Baza Fault: A major active extensional fault in the central Betic Cordillera (south Spain). *International Journal of Earth Sciences*, *97*(6), 1353–1365. https://doi.org/10.1007/s00531-007-0213-z

Alfaro, P., Sánchez-Alzola, A., Martin-Rojas, I., García-Tortosa, F. J., Galindo-Zaldívar, J., Avilés, M., et al. (2021). Geodetic fault slip rates on active faults in the Baza sub-basin (SE Spain): Insights for seismic hazard assessment. *Journal of Geodynamics*, *144*, 101815. https://doi.org/10.1016/j.jog.2021.101815

Álvarez-Gómez, J. A., Herrero-Barbero, P., & Martínez-Díaz, J. J. (2022). Seismogenic potential and tsunami threat of the strike-slip Carboneras fault in the western Mediterranean from physics-based earthquake simulations. *Natural Hazards and Earth System Sciences Discussions*, 1–26.

Banda, E., & Ansorge, J. (1980). Crustal structure under the central and eastern part of the Betic Cordillera. *Geophysical Journal International*, *63*(2), 515–532. https://doi.org/10.1111/j.1365-246x.1980.tb02635.x

Banda, E., Gallart, J., García-Dueñas, V., Dañobeitia, J. J., & Makris, J. (1993). Lateral variation of the crust in the Iberian Peninsula: New evidence from the Betic Cordillera. *Tectonophysics*, *221*(1), 53–66. https://doi.org/10.1016/0040-1951(93)90027-h

Belardinelli, M. E., Cocco, M., Coutant, O., & Cotton, F. (1999). Redistribution of dynamic stress during coseismic ruptures: Evidence for fault interaction and earthquake triggering. *Journal of Geophysical Research*, *104*(B7), 14925–14945. https://doi.org/10.1029/1999jb900094

Burgmann, R., & Dresen, G. (2008). Rheology of the lower crust and upper mantle: Evidence from rock mechanics, geodesy, and field observations. *Annual Review of Earth and Planetary Sciences*, *36*(1), 531–567. https://doi.org/10.1146/annurev.earth.36.031207.124326

Burov, E. B. (2011). Rheology and strength of the lithosphere. *Marine and Petroleum Geology*, *28*(8), 1402–1443. https://doi.org/10.1016/j.marpetgeo.2011.05.008

Cabañas, L., Rivas-Medina, A., Martínez-Solares, J., Gaspar-Escribano, J., Benito, B., Antón, R., & Ruiz-Barajas, S. (2015). Relationships between Mw and other earthquake size parameters in the Spanish IGN seismic catalog. *Pure and Applied Geophysics*, *172*(9), 2397–2410. https://doi.org/10.1007/s00024-014-1025-2

Carbonell, R., Torné, M., García-Dueñas, V., Moya, R., & Banda, E. (1995). The ESCI-Béticas: A seismic reflection image of the Betics orogen. *Revista de la Sociedad Geologica de Espana*, *8*(4), 503–512.

Chëry, J., Carretier, S., & Ritz, J.-F. (2001). Postseismic stress transfer explains time clustering of large earthquakes in Mongolia. *Earth and Planetary Science Letters*, *194*(1–2), 277–286. https://doi.org/10.1016/s0012-821x(01)00552-0

Comas Minondo, M. D. C., Canales, J. J. D., Marrón, J. Á., & Hermoso, J. I. S. (1995). Crustal reflections and structure in the Alboran Basin: Preliminary results of the ESCI-Alboran Survey. *Revista de la Sociedad Geologica de Espana*, *8*(4), 529–542.

Cotton, F., & Coutant, O. (1997). Dynamic stress variations due to shear faults in a plane-layered medium. *Geophysical Journal International*, *128*(3), 676–688. https://doi.org/10.1111/j.1365-246x.1997.tb05328.x

De la Peña, L. G., Ranero, C. R., Gràcia, E., & Booth-Rea, G. (2021). The evolution of the westernmost Mediterranean basins. *Earth-Science Reviews*, *214*, 103445. https://doi.org/10.1016/j.earscirev.2020.103445

De Larouzière, F., Bolze, J., Bordet, P., Hernandez, J., Montenat, C., & d'Estevou, P. O. (1988). The Betic segment of the lithospheric Trans-Alboran shear zone during the Late Miocene. *Tectonophysics*, *152*(1–2), 41–52. https://doi.org/10.1016/0040-1951(88)90028-5

De Lis Mancilla, F., & Diaz, J. (2015). High resolution Moho topography map beneath Iberia and Northern Morocco from receiver function analysis. *Tectonophysics*, *663*, 203–211. https://doi.org/10.1016/j.tecto.2015.06.017

De Mets, C., Iaffaldano, G., & Merkouriev, S. (2015). High-resolution Neogene and quaternary estimates of Nubia-Eurasia-North America plate motion. *Geophysical Journal International*, *203*(1), 416–427. https://doi.org/10.1093/gji/ggv277

Deng, J., & Sykes, L. R. (1996). Triggering of 1812 Santa Barbara earthquake by a great San Andreas shock: Implications for future seismic hazards in southern California. *Geophysical Research Letters*, *23*(10), 1155–1158. https://doi.org/10.1029/96gl00738

De Pro-Díaz, Y., Martínez-Díaz, J. J., & Catalán, C. C. (2023). The 1804 Dalías earthquake: Ranking seismic sources with the boxer and seismic scenario methods in SE Iberia. In *EGU general assembly conference abstracts* (p. 14995). https://doi.org/10.5194/egusphere-egu23-14995

Diaz, J., Torné, M., Vergés, J., Jimenez-Munt, I., Martí, J., Carbonell, R., et al. (2021). Four decades of geophysical research on Iberia and adjacent margins. *Earth-Science Reviews*, *222*, 103841. https://doi.org/10.1016/j.earscirev.2021.103841

Fernàndez, M., Marzán, I., Correia, A., & Ramalho, E. (1998). Heat flow, heat production, and lithospheric thermal regime in the Iberian Peninsula. *Tectonophysics*, *291*(1–4), 29–53. https://doi.org/10.1016/s0040-1951(98)00029-8

Fernández-Ibáñez, F., & Soto, J. (2008). Crustal rheology and seismicity in the Gibraltar Arc (western Mediterranean). *Tectonics*, *27*(2), TC2007. https://doi.org/10.1029/2007tc002192

Freed, A. M. (2007). Afterslip (and only afterslip) following the 2004 Parkfield, California, earthquake. *Geophysical Research Letters*, *34*(6), L06312. https://doi.org/10.1029/2006gl029155

Freed, A. M., Bürgmann, R., Calais, E., Freymueller, J., & Hreinsdóttir, S. (2006). Implications of deformation following the 2002 Denali, Alaska, earthquake for postseismic relaxation processes and lithospheric rheology. *Journal of Geophysical Research*, *111*(B1), B01401. https://doi.org/10.1029/2005jb003894

Freed, A. M., & Lin, J. (2001). Delayed triggering of the 1999 Hector Mine earthquake by viscoelastic stress transfer. *Nature*, *411*(6834), 180–183. https://doi.org/10.1038/35075548

García-Dueñas, V., Banda, E., Torné, M., Córdoba, D., & ESCI-Béticas Working Group. (1994). A deep seismic reflection survey across the Betic Chain (southern Spain): First results. *Tectonophysics*, *232*(1–4), 77–89. https://doi.org/10.1016/0040-1951(94)90077-9

García-Mayordomo, J. (2005). *Caracterización y análisis de la peligrosidad sísmica en el sureste de España* (Doctoral dissertation). Universidad Complutense de Madrid. Retrieved from https://www.fundaciongarciasineriz.es/wp-content/uploads/attachments/JGarcia.pdf

García-Mayordomo, J., Insua-Arévalo, J. M., Martínez-Díaz, J. J., Jiménez-Díaz, A., Martín-Banda, R., Martín-Alfageme, S., et al. (2012). The Quaternary active faults database of Iberia (QAFI v. 2.0). *Journal of Iberian Geology*, *38*(1), 285–302. https://doi.org/10.5209/rev_jige.2012.v38.n1.39219

García-Mayordomo, J., Martín-Banda, R., Insua-Arévalo, J. M., Álvarez-Gómez, J. A., Martínez-Díaz, J. J., & Cabral, J. (2017). Active fault databases: Building a bridge between earthquake geologists and seismic hazard practitioners, the case of the QAFI v. 3 database. *Natural Hazards and Earth System Sciences*, *17*(8), 1447–1459. https://doi.org/10.5194/nhess-17-1447-2017

García-Tortosa, F. J., Sanz de Galdeano, C., Alfaro, P., Galindo-Zaldívar, J., & Peláez, J. A. (2007). La falla y los pliegues de Galera. In C. Sanz de Galdeano & J. A. Peláez (Eds.), *La cuenca de Guadix-Baza: Estructura, tectónica activa, sismicidad, geomorfología y dataciones existentes* (pp. 141–153). Universidad de Granada.

García-Tortosa, F. J., & Silva, P. (2017). The 1531 Baza earthquake. In P. G. Silva & M. A. Rodríguez-Pascua (Eds.), *The catalogue of earthquake geological effects in Spain* (2nd ed., p. 806). IGME and AEQUA. (Revised and Expanded).

Gomberg, J., Beeler, N., Blanpied, M., & Bodin, P. (1998). Earthquake triggering by transient and static deformations. *Journal of Geophysical Research*, *103*(B10), 24411–24426. https://doi.org/10.1029/98jb01125

Gómez-Novell, O. (2021). *Paleoseismic transect across the Alhama de Murcia Fault and implications of a fault-based seismic hazard assessment for the Eastern Betics* (Doctoral dissertation). Universitat de Barcelona. Retrieved from http://hdl.handle.net/2445/183755

Gómez-Novell, O., Ortuño, M., García-Mayordomo, J., Insua-Arévalo, J., Rockwell, T., Baize, S., et al. (2022). Improved geological slip rate estimations in the complex Alhama de Murcia Fault zone (SE Iberia) and its implications for fault behavior. *Tectonics*, *41*(12), e2022TC007465. https://doi.org/10.1029/2022tc007465

González, Á. (2017). The Spanish national earthquake catalogue: Evolution, precision and completeness. *Journal of Seismology*, *21*(3), 435–471. https://doi.org/10.1007/s10950-016-9610-8

Hanks, T. C., & Kanamori, H. (1979). A moment magnitude scale. *Journal of Geophysical Research*, *84*(B5), 2348–2350. https://doi.org/10.1029/jb084ib05p02348

Harris, R. A. (1998). Introduction to special section: Stress triggers, stress shadows, and implications for seismic hazard. *Journal of Geophysical Research*, *103*(B10), 24347–24358. https://doi.org/10.1029/98jb01576

Harris, R. A., & Simpson, R. W. (1992). Changes in static stress on southern California faults after the 1992 Landers earthquake. *Nature*, *360*(6401), 251–254. https://doi.org/10.1038/360251a0

Hill, D. P., Reasenberg, P., Michael, A., Arabaz, W., Beroza, G., Brumbaugh, D., et al. (1993). Seismicity remotely triggered by the magnitude 7.3 Landers, California, earthquake. *Science*, *260*(5114), 1617–1623. https://doi.org/10.1126/science.260.5114.1617

Hirth, G., & Kohlstedf, D. (2003). Rheology of the upper mantle and the mantle wedge: A view from the experimentalists. *Geophysical Monograph-American Geophysical Union*, *138*, 83–106.

Hornbach, M. J., Braudy, N., Briggs, R. W., Cormier, M. H., Davis, M. B., Diebold, J. B., et al. (2010). High tsunami frequency as a result of combined strike-slip faulting and coastal landslides. *Nature Geoscience*, *3*(11), 783–788. https://doi.org/10.1038/ngeo975

Huerta, P., & Silva, P. G. (2014). The 1522 Alhama de Almería earthquake. In P. G. Silva & M. A. Rodríguez-Pascua (Eds.), *The catalogue of earthquake geological effects in Spain* (2nd ed., p. 806). IGME and AEQUA. (Revised and Expanded).

Hunter, J. D. (2007). Matplotlib: A 2D graphics environment. *Computing in Science & Engineering*, *9*(3), 90–95. https://doi.org/10.1109/mcse.2007.55

IGME. (2015). ZESIS: Base de Datos de Zonas Sismogénicas de la Península Ibérica y territorios de influencia para el cálculo de la peligrosidad sísmica en España [Dataset]. Retrieved from http://info.igme.es/zesis

IGME. (2022). QAFI: Quaternary active faults database of Iberia [Dataset]. Retrieved from https://info.igme.es/QAFI

IGN. (2022). National geographic Institute (IGN) Spanish seismic catalog [Dataset]. https://doi.org/10.7419/162.03.2022

IGN, & UPM. (2013). *Actualización de mapas de peligrosidad sísmica de España*. Editorial Centro Nacional de Información Geográfica.

Jia, Z., Jin, Z., Marchandon, M., Ulrich, T., Gabriel, A.-A., Fan, W., et al. (2023). The complex dynamics of the 2023 Kahramanmaraş, Turkey, Mw 7.8-7.7 earthquake doublet. *Science*, *381*(6661), 985–990. https://doi.org/10.1126/science.adi0685

Jin, Z., Fialko, Y., Yang, H., & Li, Y. (2023). Transient deformation excited by the 2021 M7.4 Maduo (China) earthquake: Evidence of a deep shear zone. *Journal of Geophysical Research: Solid Earth*, *128*(8), e2023JB026643. https://doi.org/10.1029/2023jb026643

Kilb, D., Gomberg, J., & Bodin, P. (2000). Earthquake triggering by dynamic stresses. *Nature*, *408*(6812), 570–574. https://doi.org/10.1038/35046046

King, G. C. P., & Cocco, M. (2001). Fault interaction by elastic stress changes: New clues from earthquake sequences. *Advances in Geophysics*, *44*, 1–VIII. https://doi.org/10.1016/S0065-2687(00)80006-0

King, G. C. P., Stein, R. S., & Lin, J. (1994). Static stress changes and the triggering of earthquakes. *Bulletin of the Seismological Society of America*, *84*(3), 935–953.

Liu, L., Li, Y., Ji, L., & Zhu, L. (2022). Finite element simulation of stress change for the MS7. 4 Madoi earthquake and implications for regional seismic hazards. *Earthquake Research Advances*, *2*(2), 100046. https://doi.org/10.1016/j.eqrea.2021.100046

López-Escudero, R., Masana, E., Khazaradze, G., Gómez-Novell, O., Pallàs, R., Ortuño, M., et al. (2019). Refining seismic parameters of the Carboneras fault (SE Iberia) from late Pleistocene to early Holocene at Tostana site. In J. García-Mayordomo, L. Peruzza, M. Ortuño, B. Pace, & O. Scotti (Eds.), *Proceedings of the 4 Fault2SHA workshop: Fault complex interaction, 3-5 June 2019* (p. 23).

López-Escudero, R., Masana, E., Khazaradze, G., Pallàs, R., Gómez-Novell, O., Ortuño, M., et al. (2018). Paleoseismic investigations of the Carboneras Fault (SE Iberia): First trenching results at Tostana site. In *EGU general assembly conference abstracts* (p. 9650).

Marchandon, M., Vergnolle, M., & Cavalié, O. (2021). Fault interactions in a complex fault system: Insight from the 1936–1997 NE Lut earthquake sequence. *Geophysical Journal International*, *224*(2), 1157–1173. https://doi.org/10.1093/gji/ggaa451

Marco, S., Stein, M., Agnon, A., & Ron, H. (1996). Long-term earthquake clustering: A 50,000-year paleoseismic record in the Dead Sea Graben. *Journal of Geophysical Research*, *101*(B3), 6179–6191. https://doi.org/10.1029/95jb01587

Marone, C. J., Scholtz, C., & Bilham, R. (1991). On the mechanics of earthquake afterslip. *Journal of Geophysical Research*, *96*(B5), 8441–8452. https://doi.org/10.1029/91jb00275

Martínez-Díaz, J. J., Alonso-Henar, J., Insua-Arévalo, J. M., Canora, C., García-Mayordomo, J., Rodríguez-Escudero, E., et al. (2019). Geological evidences of surface rupture related to a seventeenth century destructive earthquake in Betic Cordillera (SE Spain): Constraining the seismic hazard of the Alhama de Murcia fault. *Journal of Iberian Geology*, *45*(1), 73–86. https://doi.org/10.1007/s41513-018-0082-2

Martínez-Díaz, J. J., Bejar-Pizarro, M., Álvarez-Gómez, J. A., De Lis Mancilla, F., Stich, D., Herrera, G., & Morales, J. (2012). Tectonic and seismic implications of an intersegment rupture: The damaging May 11th 2011 Mw 5.2 Lorca earthquake, Spain. *Tectonophysics*, *546*, 28–37. https://doi.org/10.1016/j.tecto.2012.04.010

Martínez Díaz, J. J., Masana, E., & Ortuño, M. (2012). Active tectonics of the Alhama de Murcia fault, Betic Cordillera, Spain. *Journal of Iberian Geology*, *38*(1), 253–270. https://doi.org/10.5209/rev_jige.2012.v38.n1.39218

Martınez-Solares, J. M., & Mezcua, J. (2002). *Catálogo sísmico de la Península Ibérica:(880 a. C-1900) (Monografía núm* (18th ed.). Ministerio de Fomento, Instituto Geográfico Nacional.

Masana, E., Moreno, X., Gràcia, E., Pallàs, R., Ortuño, M., López, R., et al. (2018). First evidence of paleoearthquakes along the Carboneras fault zone (SE Iberian Peninsula): Los Trances site. *Geológica Acta*, 461–476.

Medina-Cascales, I. (2021). *Geometry, kinematics and palaeoseismology of the Baza and Galera fault zones (Guadix-Baza basin, Betic Cordillera)* (Doctoral dissertation). Universidad de Alicante. Retrieved from http://hdl.handle.net/10045/129273

Medina-Cascales, I., García-Tortosa, F. J., Martin-Rojas, I., Pérez-Peña, J. V., & Alfaro, P. (2021). Tectonic geomorphology of an active slow-moving, intrabasinal fault: The Galera Fault (Guadix-Baza Basin, central Betic Cordillera, southern Spain). *Geomorphology*, *393*, 107941. https://doi.org/10.1016/j.geomorph.2021.107941

Medina-Cascales, I., Martin-Rojas, I., García-Tortosa, F. J., Peláez, J. A., & Alfaro, P. (2020). Geometry and kinematics of the Baza Fault (central Betic Cordillera, South Spain): Insights into its seismic potential. *Geológica Acta*, *18*(11), 1–25. https://doi.org/10.1344/GeologicaActa2020.18.11

Mezcua, J., Rueda, J., & Blanco, R. M. G. (2004). Reevaluation of historic earthquakes in Spain. *Seismological Research Letters*, *75*(1), 75–81. https://doi.org/10.1785/gssrl.75.1.75

Mohammadi, H. (2022). Possible influence of static and viscoelastic stress perturbations in Musgrave block (Central Australia) earthquake sequence. *Physics of the Earth and Planetary Interiors*, *322*, 106830. https://doi.org/10.1016/j.pepi.2021.106830

Molins-Vigatà, J., García-Mayordomo, J., Ortuño, M., García-Sellés, D., & Gómez-Novell, O. (2022). Caracterización geológica de la falla del Llano del Águila en Campo Dalías (Almería): Posible fuente sismogénica del terremoto de 1804. *Revista de la Sociedad Geologica de Espana*, *35*(1), 71–83. https://doi.org/10.55407/rsge.94908

Morales, J., Molina-Aguilera, A., de Lis Mancilla, F., Stich, D., Azañón, J. M., Teixidó, T., et al. (2022). Preservation of the Iberian Tethys paleomargin beneath the eastern Betic mountain range. *Gondwana Research*, *106*, 237–246. https://doi.org/10.1016/j.gr.2022.01.015

Moreno, X. (2010). *Neotectonic and paleoseismic onshore-offshore integrated study of the Carboneras Fault (Eastern Betics, SE Iberia)* (Doctoral dissertation). Universitat de Barcelona. Retrieved from http://hdl.handle.net/10803/77873

Moreno, X., Masana, E., Pallàs, R., Gràcia, E., Rodés, Á., & Bordonau, J. (2015). Quaternary tectonic activity of the Carboneras Fault in the La Serrata range (SE Iberia): Geomorphological and chronological constraints. *Tectonophysics*, *663*, 78–94. https://doi.org/10.1016/j.tecto.2015.08.016

Murphy, P. (2019). Los terremotos de Almería de 1804. In *El archivo histórico nacional*. Instituto Geográfico Nacional.

Nalbant, S. S., Hubert, A., & King, G. C. (1998). Stress coupling between earthquakes in northwest Turkey and the north Aegean sea. *Journal of Geophysical Research*, *103*(B10), 24469–24486. https://doi.org/10.1029/98jb01491

Negredo, A., De Lis Mancilla, F., Clemente, C., Morales, J., & Fullea, J. (2020). Geodynamic modelling of edge-delamination driven by STEP faults: The westernmost Mediterranean margin (central Betic orogen) case study. *Frontiers in Earth Science*, *8*, 435. https://doi.org/10.3389/feart.2020.533392

Nur, A., & Cline, E. H. (2000). Poseidon's horses: Plate tectonics and earthquake storms in the late bronze Age Aegean and eastern Mediterranean. *Journal of Archaeological Science*, *27*(1), 43–63. https://doi.org/10.1006/jasc.1999.0431

Nur, A., & Mavko, G. (1974). Postseismic viscoelastic rebound. *Science*, *183*(4121), 204–206. https://doi.org/10.1126/science.183.4121.204

Palano, M., González, P. J., & Fernández, J. (2015). The diffuse plate boundary of Nubia and Iberia in the Western Mediterranean: Crustal deformation evidence for viscous coupling and fragmented lithosphere. *Earth and Planetary Science Letters*, *430*, 439–447. https://doi.org/10.1016/j.epsl.2015.08.040

Parsons, T., Ji, C., & Kirby, E. (2008). Stress changes from the 2008 Wenchuan earthquake and increased hazard in the Sichuan basin. *Nature*, *454*(7203), 509–510. https://doi.org/10.1038/nature07177

Pedrera, A., Galindo-Zaldívar, J., Marín-Lechado, C., García-Tortosa, F., Ruano, P., López Garrido, A., et al. (2012). Recent and active faults and folds in the central-eastern Internal Zones of the Betic Cordillera/las fallas y pliegues recientes y activos de la parte centro-oriental de las zonas internas de la Cordillera Bética. *Journal of Iberian Geology*, *38*(1), 191–208. https://doi.org/10.5209/rev_jige.2012.v38.n1.39213

Pollitz, F. F., & Sacks, I. S. (1995). Consequences of stress changes following the 1891 Nobi earthquake, Japan. *Bulletin of the Seismological Society of America*, *85*(3), 796–807.

Pollitz, F. F., & Sacks, I. S. (1997). The 1995 Kobe, Japan, earthquake: A long-delayed aftershock of the offshore 1944 Tonankai and 1946 Nankaido earthquakes. *Bulletin of the Seismological Society of America*, *87*(1), 1–10. https://doi.org/10.1785/bssa0870010001

Polyak, B., Fernàndez, M., Khutorskoy, M., Soto, J., Basov, I., Comas, M., et al. (1996). Heat flow in the Alboran Sea, western Mediterranean. *Tectonophysics*, *263*(1–4), 191–218. https://doi.org/10.1016/0040-1951(95)00178-6

Pondard, N., Armijo, R., King, G. C., Meyer, B., & Flerit, F. (2007). Fault interactions in the Sea of Marmara pull-apart (North Anatolian Fault): Earthquake clustering and propagating earthquake sequences. *Geophysical Journal International*, *171*(3), 1185–1197. https://doi.org/10.1111/j.1365-246x.2007.03580.x

Poort, J., Lucazeau, F., Le Gal, V., Dal Cin, M., Leroux, E., Bouzid, A., et al. (2020). Heat flow in the Western Mediterranean: Thermal anomalies on the margins, the seafloor and the transfer zones. *Marine Geology*, *419*, 106064. https://doi.org/10.1016/j.margeo.2019.106064

QGIS Development Team. (2021). QGIS geographic information system [Software]. Retrieved from https://www.qgis.org

Ranalli, G. (1995). *Rheology of the Earth*. Springer Science & Business Media.

Reasenberg, P. A., & Simpson, R. W. (1992). Response of regional seismicity to the static stress change produced by the Loma Prieta earthquake. *Science*, *255*(5052), 1687–1690. https://doi.org/10.1126/science.255.5052.1687

Reicherter, K., & Becker-Heidmann, P. (2009). Tsunami deposits in the western Mediterranean: Remains of the 1522 Almería earthquake? *Geological Society, London, Special Publications*, *316*(1), 217–235. https://doi.org/10.1144/sp316.14

Reicherter, K., & Hübscher, C. (2007). Evidence for a seafloor rupture of the Carboneras Fault Zone (southern Spain): Relation to the 1522 Almería earthquake? *Journal of Seismology*, *11*(1), 15–26. https://doi.org/10.1007/s10950-006-9024-0

Rydelek, P. A., & Sacks, I. S. (1990). Asthenospheric viscosity and stress diffusion: A mechanism to explain correlated earthquakes and surface deformations in NE Japan. *Geophysical Journal International*, *100*(1), 39–58. https://doi.org/10.1111/j.1365-246x.1990.tb04566.x

Rydelek, P. A., & Sacks, I. S. (2001). Migration of large earthquakes along the San Jacinto fault; stress diffusion from the 1857 Fort Tejon earthquake. *Geophysical Research Letters*, *28*(16), 3079–3082. https://doi.org/10.1029/2001gl013005

Santoyo, M. A., Singh, S. K., Mikumo, T., & Ordaz, M. (2005). Space–time clustering of large thrust earthquakes along the Mexican subduction zone: An evidence of source stress interaction. *Bulletin of the Seismological Society of America*, *95*(5), 1856–1864. https://doi.org/10.1785/0120040185

Sanz de Galdeano, C., Azañón, J. M., Cabral, J., Ruano, P., Alfaro, P., Canora, C., et al. (2019). Active faults in Iberia. In C. Quesada & J. Oliveira (Eds.), *The geology of Iberia: A geodynamic approach: Volume 5: Active processes: Seismicity, active faulting and relief* (pp. 33–75). Springer. https://doi.org/10.1007/978-3-030-10931-8_4

Sanz de Galdeano, C., & Vera, J. A. (1992). Stratigraphic record and palaeogeographical context of the Neogene basins in the Betic Cordillera, Spain. *Basin Research*, *4*(1), 21–36. https://doi.org/10.1111/j.1365-2117.1992.tb00040.x

Scholz, C. H. (2019). *The mechanics of earthquakes and faulting*. Cambridge University Press.

Segou, M., & Parsons, T. (2020). A new technique to calculate earthquake stress transfer and to probe the physics of aftershocks. *Bulletin of the Seismological Society of America*, *110*(2), 863–873. https://doi.org/10.1785/0120190033

Silva, P. G. (2017). The 1658 Almería earthquake. In P. G. Silva & M. A. Rodríguez-Pascua (Eds.), *The catalogue of earthquake geological effects in Spain* (2nd ed., p. 806). IGME and AEQUA. (Revised and Expanded).

Silva, P. G., Goy, J. L., Somoza, L., Zazo, C., & Bardají, T. (1993). Landscape response to strike-slip faulting linked to collisional settings: Quaternary tectonics and basin formation in the Eastern Betics, southeastern Spain. *Tectonophysics*, *224*(4), 289–303. https://doi.org/10.1016/0040-1951(93)90034-h

Silva, P. G., Rodríguez-Pascua, M. A., Giner Robles, J. L., Élez, J., Huerta, P., García-Tortosa, F. J., et al. (2019). *Catálogo de los efectos geológicos de los terremotos en España. 2. ª Edición (Revisada y ampliada). Serie Riesgos Geológicos y Geotecnia nº 6*. Instituto Geológico y Minero de España (IGME).

Silva, P. G., & Roquero, E. (2017). The 1518 Vera earthquake. In P. G. Silva & M. A. Rodríguez-Pascua (Eds.), *The catalogue of earthquake geological effects in Spain* (2nd ed., p. 806). IGME and AEQUA. (Revised and Expanded).

Soto, J. I., Fernández-Ibáñez, F., Fernandez, M., & García-Casco, A. (2008). Thermal structure of the crust in the Gibraltar Arc: Influence on active tectonics in the western Mediterranean. *Geochemistry, Geophysics, Geosystems*, *9*(10), Q10011. https://doi.org/10.1029/2008gc002061

Stacey, F. D., & Davis, P. M. (1977). *Physics of the Earth* (Vol. 2). Wiley.

Stein, R. S. (1999). The role of stress transfer in earthquake occurrence. *Nature*, *402*(6762), 605–609. https://doi.org/10.1038/45144

Stein, R. S., Barka, A. A., & Dieterich, J. H. (1997). Progressive failure on the North Anatolian fault since 1939 by earthquake stress triggering. *Geophysical Journal International*, *128*(3), 594–604. https://doi.org/10.1111/j.1365-246x.1997.tb05321.x

Sunbul, F. (2019). Time-dependent stress increase along the major faults in eastern Turkey. *Journal of Geodynamics*, *126*, 23–31. https://doi.org/10.1016/j.jog.2019.03.001

Tendero-Salmerón, V., Galindo-Zaldivar, J., d'Acremont, E., Catalán, M., Martos, Y. M., Ammar, A., & Ercilla, G. (2022). New insights on the Alboran Sea basin extension and continental collision from magnetic anomalies related to magmatism (western Mediterranean). *Marine Geology*, *443*, 106696. https://doi.org/10.1016/j.margeo.2021.106696

Tesauro, M., Burov, E. B., Kaban, M. K., & Cloetingh, S. A. (2011). Ductile crustal flow in Europe's lithosphere. *Earth and Planetary Science Letters*, *312*(1–2), 254–265. https://doi.org/10.1016/j.epsl.2011.09.055

Toda, S., Lin, J., & Stein, R. S. (2011). Using the 2011 Mw 9.0 off the Pacific coast of Tohoku Earthquake to test the Coulomb stress triggering hypothesis and to calculate faults brought closer to failure. *Earth Planets and Space*, *63*(7), 725–730. https://doi.org/10.5047/eps.2011.05.010

Toda, S., & Stein, R. S. (2020). Long-and short-term stress interaction of the 2019 Ridgecrest sequence and Coulomb-based earthquake forecasts. *Bulletin of the Seismological Society of America*, *110*(4), 1765–1780. https://doi.org/10.1785/0120200169

Torne, M., Fernàndez, M., Vergés, J., Ayala, C., Salas, M. C., Jimenez-Munt, I., et al. (2015). Crust and mantle lithospheric structure of the Iberian Peninsula deduced from potential field modeling and thermal analysis. *Tectonophysics*, *663*, 419–433. https://doi.org/10.1016/j.tecto.2015.06.003

Torne, M., Jiménez-Munt, I., Negredo, A., Fullea, J., Vergés, J., Marzán, I., et al. (2023). Advances in the modeling of the Iberian thermal lithosphere and perspectives on deep geothermal studies. *Geothermal Energy*, *11*(1), 1–25. https://doi.org/10.1186/s40517-023-00246-6

Turcotte, D. L., & Schubert, G. (2002). *Geodynamics*. Cambridge University Press.

Verdecchia, A., Pace, B., Visini, F., Scotti, O., Peruzza, L., & Benedetti, L. (2018). The role of viscoelastic stress transfer in long-term earthquake cascades: Insights after the central Italy 2016–2017 seismic sequence. *Tectonics*, *37*(10), 3411–3428. https://doi.org/10.1029/2018tc005110

Wang, R. (2006). PSGRN/PSCMP backend for Pyrocko's Green's function manager Fomosto: Code to calculate synthetic stress/strain/tilt/gravitational fields on a layered viscoelastic halfspace [Software]. Retrieved from https://git.pyrocko.org/pyrocko/fomosto-psgrn-pscmp

Wang, R., Lorenzo-Martín, F., & Roth, F. (2006). PSGRN/PSCMP—A new code for calculating co-and post-seismic deformation, geoid and gravity changes based on the viscoelastic-gravitational dislocation theory. *Computers & Geosciences*, *32*(4), 527–541. https://doi.org/10.1016/j.cageo.2005.08.006

Weijermars, R. (1987). The Palomares brittle—Ductile shear zone of southern Spain. *Journal of Structural Geology*, *9*(2), 139–157. https://doi.org/10.1016/0191-8141(87)90022-8

Wells, D. L., & Coppersmith, K. J. (1994). New empirical relationships among magnitude, rupture length, rupture width, rupture area, and surface displacement. *Bulletin of the Seismological Society of America*, *84*(4), 974–1002. https://doi.org/10.1785/bssa0840040974

Xiong, X., Shan, B., Zhou, Y., Wei, S., Li, Y., Wang, R., & Zheng, Y. (2017). Coulomb stress transfer and accumulation on the Sagaing Fault, Myanmar, over the past 110 years and its implications for seismic hazard. *Geophysical Research Letters*, *44*(10), 4781–4789. https://doi.org/10.1002/2017gl072770

Yazdi, P. (2019). *Analysis of earthquake sequences and activity rates: Implications for seismic hazard* (Doctoral dissertation). Universidad Politécnica de Madrid. https://doi.org/10.20868/UPM.thesis.58691

Zohar, M., Salamon, A., & Rubin, R. (2017). Earthquake damage history in Israel and its close surrounding-evaluation of spatial and temporal patterns. *Tectonophysics*, *696*, 1–13. https://doi.org/10.1016/j.tecto.2016.12.015